International Space Planes and Hypersonic Systems and Technologies Conferences
6-9 July 2015, Glasgow, Scotland
20th AIAA International Space Planes and Hypersonic Systems and Technologies Conference

A Conceptual Design of Next Generation Hypersonic Air-breathing Airplanes with Dual Waveriders Forebody

Kai Cui[1], Shou-Chao Hu[2], Guang-li Li[3], Yao Xiao[4]

State Key Laboratory of High Temperature Gas Dynamics, Institute of Mechanics, Chinese Academy of Sciences, Beijing 100190, China

and

Ming Situ[5]

The 31th Research Institute of CASIC, Beijing, 100074, China

A design methodology employed for a practical preliminary-level integration of next generation hypersonic airplanes is presented in this paper. The key feature of this type of configurations is that the forebody of the vehicle is designed by rotating and assembling two waverider-based-surfaces, which are defined by linear edges. The propulsion system assumes two scramjets with cylindrical combustion chambers. The layout of the configuration presents a Blend-Wing-Body aircraft in order to integrate the airframe and the propulsion units as well as to improve the aerodynamic performance. A 7.2 m long, Mach 6 vehicle is presented, and multi-point aerodynamic performance predictions are carried out by using computational fluid dynamics with a fully turbulent model at the flight Mach numbers range from 4 to 7, the flight angles of attack range from 0 to 8 degree, and the flight altitudes range from 20 km to 29 km. Numerical results demonstrates that such a design of the forebody could produce a good quality flowfield for the scramjets. Moreover, a relatively high lift-to-drag ratio can be obtained. The maximal values vary from 3.75 to 3.31 when the flight Mach number/altitude vary from 4/20 km to 7/29 km.

Nomenclature

C_l = Lift coefficient
C_d = Drag coefficient
C_{my} = Pitching moment coefficient
D = Drag
H = Gap width, flight height
L = Length, lift
Ma = Mach number
P_s = Static pressure
S_p = Projective area in vertical direction
W = Wingspan
X_{cp} = Longitudinal pressure center coefficient
V = Volume
α = Rotation angle, flight angle of attack
α_i = Wedge angle
α_r = Bending angle
δ = Total pressure recovery coefficient

---

[1] Associate Professor, LHD of Institute of Mechanics, CAS, Haidian, Beijing,100190, China, kcui@imech.ac.cn.
[2] Graduate Student, LHD of Institute of Mechanics, CAS, Haidian, Beijing,100190, China.
[3] Graduate Student, LHD of Institute of Mechanics, CAS, Haidian, Beijing,100190, China.
[4] Graduate Student, LHD of Institute of Mechanics, CAS, Haidian, Beijing,100190, China.
[5] Professor, The 31th Research Institute of CASIC, Yungang, Beijing, 100074, China

η_v	=	Volumetric efficiency
ρ	=	Density
δ	=	Total pressure recovery coefficient

Subscripts

B	=	whole configuration
f	=	forebody
i	=	inlet
c	=	compressing section

I. Introduction

Air-breathing hypersonic flight vehicles powered by scramjets had been of much concern in recent decades[1]. Hypersonic vehicles could be used in many fields, such as high-speed strike weapons and reused carriers to access the space[2-4]. Hypersonic airplanes[5] that transport passengers and cargoes should also be one of the most important applications in future. Since the waverider-based airframe-engine integrated design has been deemed as the most competitive candidates of hypersonic vehicle configurations, a lot of related studies had been carried out from 1990s. Because there is no flow spillage from the lower surface to the upper surface, a waverider could obtain a large lift-to-drag ratio (*L/D*) as well as a uniformly compressed flowfield for the inlet of the scramjet. Naturally, the ventral intake layout by using a waverider as the forebody and by placing scramjets beneath the vehicle has aroused great concern of scientists and engineers[6-18].

O'Neill and Lewis[6] presented several engine-airframe integrated vehicles based on waverider configurations that generated from conical flowfields. They also carried out a series of optimization studies. The product of the *L/D* and the specific impulse was taken as the objective for a cruiser; and then the objective was replaced by the effective specific impulse for an accelerator[10]. Afterwards, Takashima and Lewis[11, 12] selected a hybrid wedge-cone combinational shape as the generating body to generate a better waverider forebody, and the *L/D* of the vehicle was maximized by using optimization routines. Cui and Yang[17] proposed a conceptual configuration by applying a similar design philosophy. In their study, a waverider generated from an elliptical cone flowfield was adopted as a baseline model, and a scramjet module was embedded beneath the lower surface of the waverider. Moreover, the upper surface was devided into two parts, i.e., the wing part and the body part. The former part was designed as an expansion surface in favor of the *L/D*, while the latter part used an upwarp surface to provide a large volume.

Due to a waverider can be designed by the osculating cone method[19], this type of waverider was also introduced to design a hypersonic airplane configuration. Takashima and Lewis[15] presented an osculating cone waverider-based hypersonic vehicle and optimized for maximum cruise performance using the method of sequential quadratic programming. Where they took into account certain aspects of off-design performance, particularly the hypersonic acceleration phase. To aim at developing conceptual design method for generating hypersonic transport configurations, Lobbia and Suzuki[16] presented two civil transport aircraft configurations with 250 and 400 seats, respectively. They employed osculating cone waveriders as the basis not only to provide increased aerodynamic efficiency, but also because of the fact that the inverse design process allows the upper surface to be designed around the mission payload requirements. More recently, a further study that include several improvements incorporated into the design method to provide increased fidelity of the results and the utilization of a genetic algorithm optimization technique to more thoroughly explore the design trade space was published by them[18].

A primary shortcoming of the scramjet is that it is unable to generate static thrust (thrust at zero velocity) and have poor performance at low Mach numbers. Hence, some other engine systems (turbofan, rocket, etc.) must be integrated into the vehicle design in order for the system to reach the high speed for which it was designed. O'Brien and Lewis[20] presented an aerodynamic model for a rocket-based combined-cycle (RBCC) engine-airframe integrated vehicle using an osculating cone waverider forebody. Javaid and Serghides presented a design methodology for integrating a turbo-ramjet and scramjet[21] as well as integrating multiple engine flow paths[22] with a conically derived waverider airframe to achieve sustained hypersonic flight. It should be noted that ventral intake layouts were adopted in all above studies.

Compared with the ventral intake layout above, only a few studies were conducted for the flanking inlet layout. The HTV-3X[23, 24] was focused on addressing an extended duration, hydrocarbon-fueled, reusable hypersonic cruise vehicle. The Turbine-Based Combined Cycle (TBCC) propulsion system of HTV-3X, which employs a unique inward-turning inlet design that efficiently provides air during each engine cycle, was capable of operating from a conventional runway up to speeds greater than Mach 6. The aerodynamic configuration of the HTV-3X used a

Blend-Wing-Body (BWB) design, which evolved from the Falcon HCV waverider shape to a higher fineness ratio, slender body to reduce wave drag.

Motivated by drawing on the merits of waveriders and the dual flanking inlet BWB layout, Cui and Hu et al proposed a novel forebody design methodology which by rotating and assembling two waverider-based surfaces, and some conceptual configurations was also presented[25]. The main advantage of this layout is that the scramjets could be fully buried into the airframe; and the abdominal space of the vehicle can be fully released to contain various payloads or equipments, such as the landing gear system and the radar system. The results for forebodies analysis showed that large air mass flow, high lift-to-drag ratio, and uniformly distributed flow-field at the inlet cross-section can be assured simultaneously. However, numerical results showed that the bow shock wave zone that generated by the stitching surface between the two waveriders contaminated the flowfield downstream as well as leaded to the increase of the aerodynamic drag since a quadric curve has been adopted as the leading edge to defien the waverider surface. Besides, the propulsion system was not included in the previous study.

The main objective of this paper is to further develop the design methodology. Furthermore, a 7.2 m long, practical preliminary-level BWB hypersonic airplane configuration design with two axisymmetric scramjet engines is presented, as shown in Fig. 1. The forebody of the configuration was designed based on cone-derived waveriders, which were defined by linear leading edges to weaken the bow shock wave generated by the connection surface between the two waverider surfaces. A kind of bilateral compression inlet was presented and used to connect the forebody and the scramjet in each engine flowpath. The whole configuration was mainly composed of the body and the wings, which were stitched by smooth surfaces to retain the

Fig. 1 BWB hypersonic airplane demonstrator configuration.

feature of BWB. Multi-point aerodynamic performance predictions were carried out by using computational fluid dynamics with a fully turbulent model at the flight Mach numbers range from 4 to 7, the flight angles of attack range from 0 to 8 degree, and the flight altitudes range from 20 km to 29 km. Numerical results demonstrates that such a design of the forebody could produce a good quality flowfield for the scramjet. Moreover, the values of the maximal lift-to-drag ratio vary from 3.75 to 3.31 when the flight Mach number/altitude vary from 4/20 km to 7/29 km.
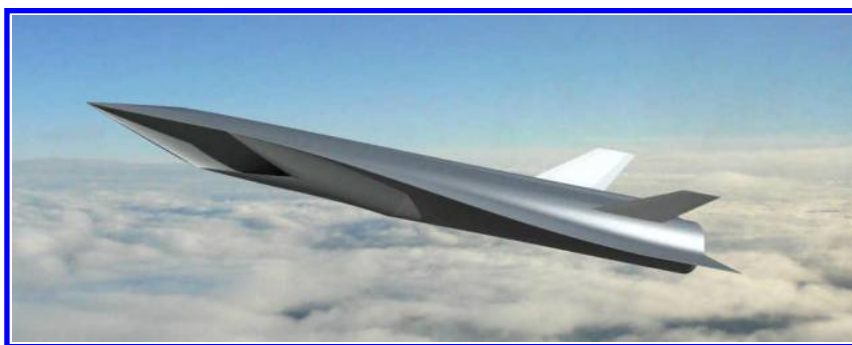
II.   Forebody Design and Evaluation

Linear leading edges were used to define waveriders in this study in order to avoid the problems stated above. A three-dimensional view and the main parts of the forebody are shown in Fig. 2. The design procedure is illustrated in Fig. 3, and a brief explanation is as follows. First of all, the baseline compression surface is generated according to the conical flowfield derived waverider design philosophy (Step A). Next, the baseline waverider is rotated along its longitudinal body axis with a pre-defined parameter, i.e., the rotation angle α (Step B). Afterwards, the rotated waverider-surface is duplicated and mirrored to generate the other compression surface, and the gap width is defined by a parameter H (Step C). Thus both the left and the right compression surfaces can be obtained to match two scramjets. Finally, the lower gap between two waveriders is sewed up by a stitching surface. The upper surface can be designed flexibly to meet the requirements of volume and aerodynamic performance. Besides, the sharp edge of the forebody needs to be blunted for thermal protection (Step D).
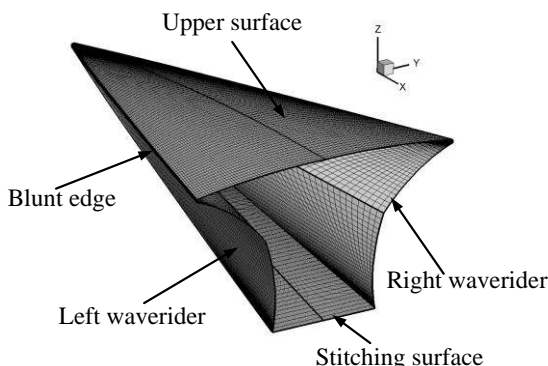

Fig. 2 Three-dimensional view of the forebody.

3
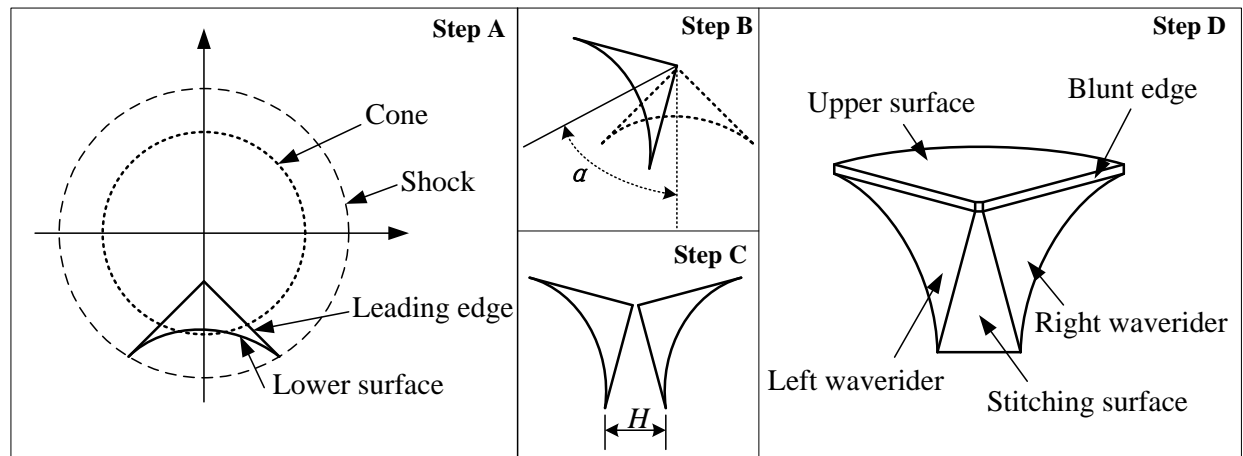American Institute of Aeronautics and Astronautics

Fig. 3 Design procedure of the forebody.

Two forebody configurations were designed and the flowfields around them were computed to examine the characteristics. A Mach 6 baseline waverider for creating the forebody was generated by using the codes GCBWRG developed by Cui et al[26, 27]. The intersection angle between the two leading edges is 90 degree. The first forebody configuration, as shown in the left figure of Fig. 4, is comprised of two waveriders that directly join at the leading edge. The rotation angle α and the gap width H are set to 45 degree and zero, respectively. In fact, the configuration can be regarded as half part of the star-body presented by Sabean and Lewis.[28] A three-dimensional Euler equations solver with unstructured grids was used as the CFD module. The flight angle of attack of the free-stream is zero degree. The grids and the pressure contour at the outlet plane are shown in the middle and the right part of Fig. 4. It is clear that the characteristic of waverider is fully retained.
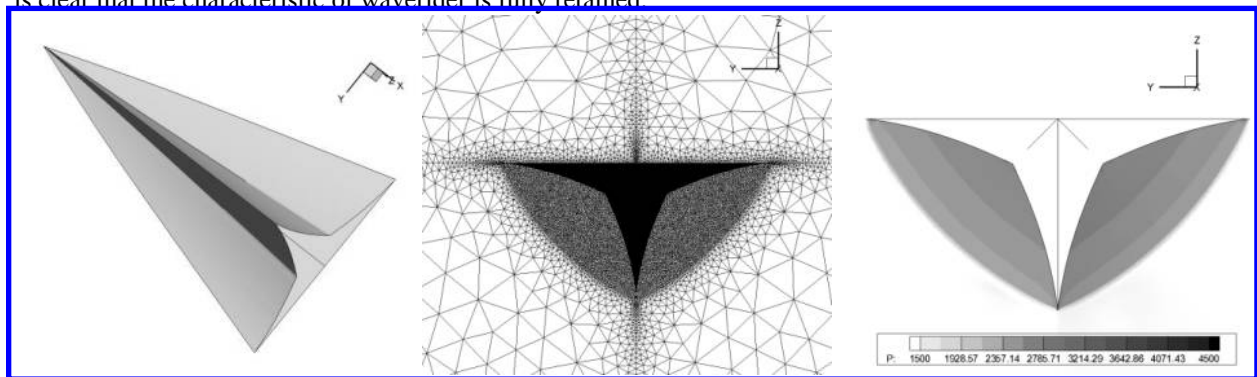

Fig. 4 The shape(left), the grids(middle), and the pressure contour at the outlet(right) of test case 1.

The second forebody configuration is the one that has been shown in Fig. 2. Unlike the first forebody configuration, the rotation angle α is set to 60 degree, hence a relatively large stitching surface is needed. The distance between the two waverider compression surfaces is large enough, which will be conductive to the arrangement of the scramjet engines. Besides, the forebody is blunted by using a strip with 10 mm height around the edge of the configuration. A Navier-Stokes equations solver with laminar model was used in this case. The Mach number contours at cross sections of $x/L_f=0.5$ and $x/L_f=1$ (the outlet of the forebody) at 0 and 6 degree attack angles are shown in Fig. 5 and Fig. 6. The results show that although the flowfield near the edges is slightly contaminated due to the existence of the stitching surface and the blunt surface, but the distribution of the Ma is relatively uniform.
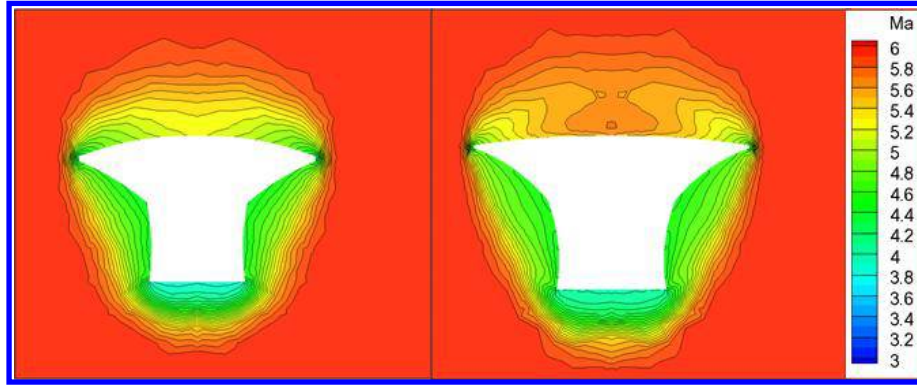
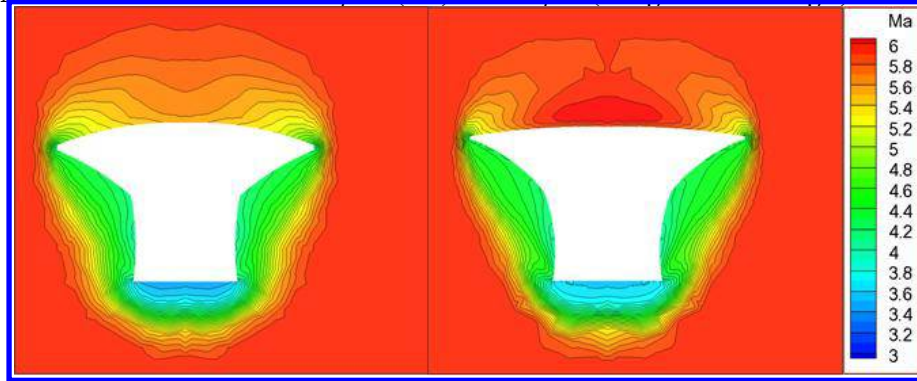**Fig. 5 Mach number contours at x/L_f=0.5(left) and x/L_f=1 (0 degree attack angle) of test case 2.**

Fig. 6 Mach number contours at x/L_f =0.5 and x/L_f =1 (6 degree attack angle) of test case 2.

III.   Design of the Vehicle

A. Inlet

Besides the waverider section, the inlet of the scramjet is comprised of the compressing section and the shrinking section, as shown in Fig. 7. The compressing section is made up of three main surfaces. The upper surface is the extension of the waverider surface to maintain the uniformity of the flowfield, and two side compression plane with wedge angle α_i (19 degree)are extra compression surfaces. The cross-sectional shape of the inlet morphs to circular through the shrinking section by using linear interpolation methods. Besides, the centerline of the shrinking section is turned to parallel to the centerline of the engine. The value of the bending angle α_r is determined by the cone angle of the generating body of the forebody.
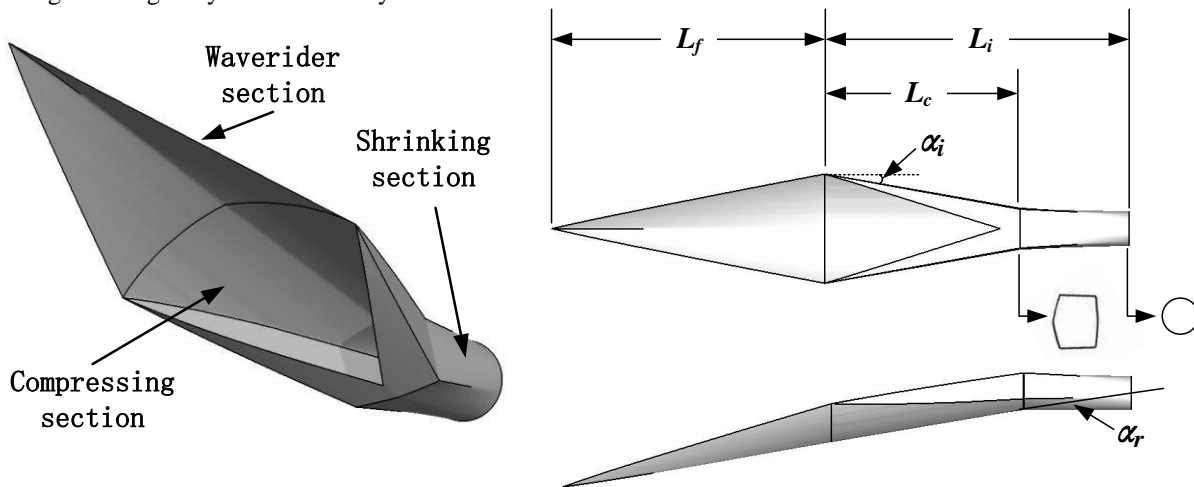

Fig. 7 The sketch of the inlet design.

5
American Institute of Aeronautics and Astronautics

B. Vehicle Configuration

The main design objective of the configuration is to pursue high aerodynamic performances, in particular a high *L/D* in small flight angle of attack, which is favorable to the operation of scramjets as well as aerodynamic drag reduction. Besides, the vehicle should provide adequate volume to contain scramjets and payloads. In order to meet the design requirements above, a BWB design methodology is adopted. The three-dimensional effect graph of the configuration has been shown in Fig. 1, and the three-view drawing is shown in Fig. 8.
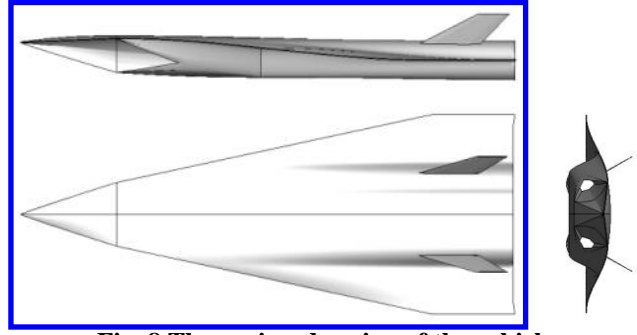
As shown in Fig. 8, the whole configuration mainly comprises of the upper and the lower surfaces.

Fig. 8 Three-view drawing of the vehicle.

All surfaces are defined by corresponding profiles in both the cross-sectional direction and the longitudinal direction. A sketch of half-model of the configuration is shown in Fig. 9. Here a brief illu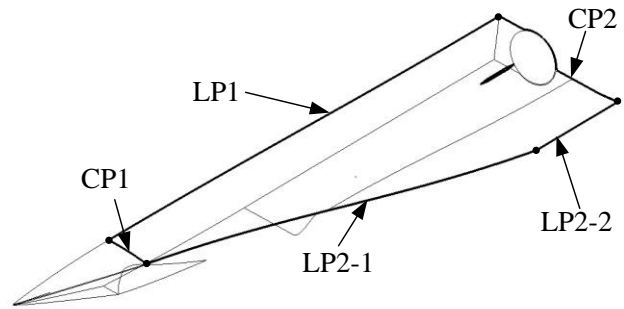stration is given by taking the upper surface of the wing-body part as an example. There are four key profile curves. Two of them are in the cross-sectional direction, i.e. CP1 and CP2, and the other two curves are in the longitudinal direction, i.e. LP1 and LP2 (connected by LP2-1 and LP 2-2). In this case a parabolic-type curve was chosen for the CP1, and the curve CP2 is connected by several lines and arc segments to fit the base shape of the vehicle in order for the base drag reduction of the vehicle. Both the curve LP1 and the curve LP2-1 are cosine curves, and the LP2-2 is a line. Once the above curves were determined, the whole surface can be generated by using interpolation methods. The whole surface is

Fig. 9 The sketch of half-model configuration.

parameterized by using such design method, and it will be very helpful for further optimization study.

There is a height difference between the start point (the intersection point between the curve CP1and the curve LP2-1) and the end point (the intersection point between the line LP2-2 and the curve CP2) of the upper surface, as shown in Fig. 9. By taken a cosine-type curve (LP1 and LP2-1) as the baseline curve, the smoothness of the surface can be guaranteed. Moreover, the wing part of the vehicle naturally deflects downward. Such type of design is contribute to the improvement of the *L/D* of the vehicle in small flight angle of attack. For the sake of further illustration, profiles in different positions at wingspan direction are shown in Fig. 10.
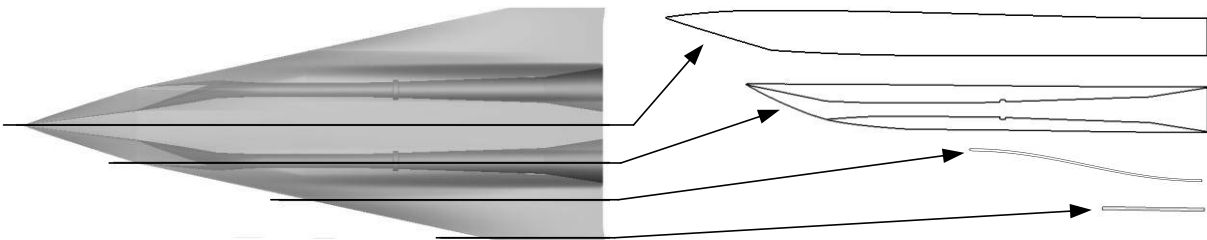

Fig. 10 Profiles at different positions.

The values of some key geometrical parameters of the final configuration are listed in Table 1, in which L_B denotes the total length of the configuration, W_B is the wingspan, L_f is the length of the forebody, V is the inner volume of the vehicle, S_p is the projective area in vertical direction, and η_v is the volumetric efficiency.

Table 1 Geometrical parameters of the configuration

L_B, m	W_B, m	L_f, m	V, m^3	S_p, m^2	$\eta_v = V^{2/3}/S_p$
7.2	2.93	1.4	5.88	12.82	0.32

IV.   Performance Evaluations of the Configuration

Numerical studies were carried out to evaluate the aerodynamic performance of the configuration by using CFD analysis. The computational domain is shown in the left figure of Fig. 11. The inner flowpath of the engine was included but it was only taken as a "cold" pipe, and without any combustion model was considered here. The whole domain were discretized by unstructured tetrahedral grids, and the total mesh number is about 10.65 million. The triangle meshes on the surface are refined to capture the boundary layer (the gird density of the surface is about 4 mm). The inviscid terms of the governing equations are approximated by the standard upwind-based flux-difference-splitting scheme of Roe, the viscous terms are discretized by the second-order central difference, and the standard K-ε model with wall function were used as the turbulent model.
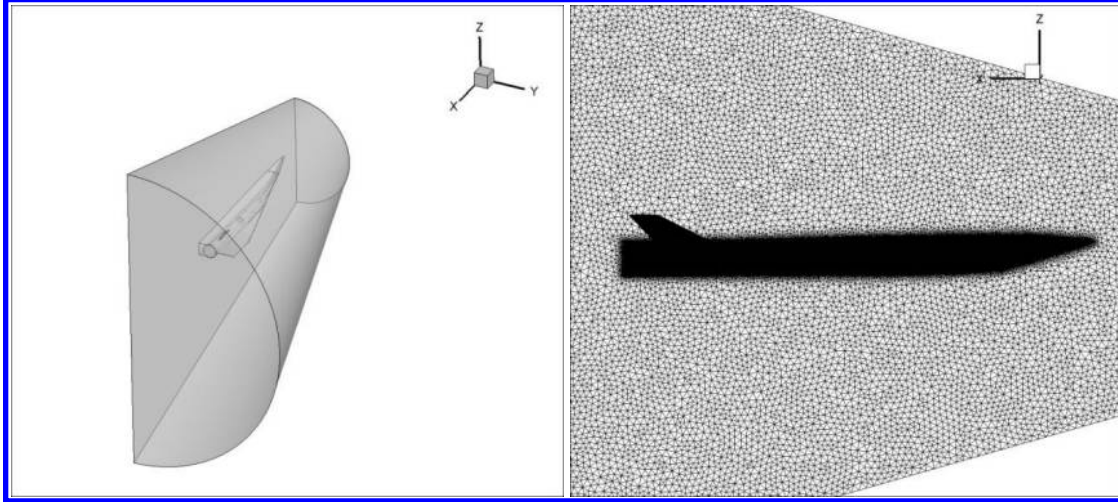

Fig. 11 Computational domain (left) and grids (right).

A. Flowfield Characteristics of the Engine Flow-path

The Mach number contours at different cross-sectional positions and the wall pressure contour on the inner flowpath of the engines at flight conditions of $Ma=6$, $H=26$ km, and $\alpha=0$ degree are shown in Fig. 12. Note from these figures that the airflow is compressed by the side walls from the entrance of the inlet and then expands when the airflow enters to the shrinking section. Thus the air pressure increases first and then decreases. Afterwards, the airflow is compressed again by a series of reflected shocks in the isolator and results in a gradually increase of the pressure. On the other hand, these figures also show that the Mach number distribution is relative uniform in different cross-sectional positions.
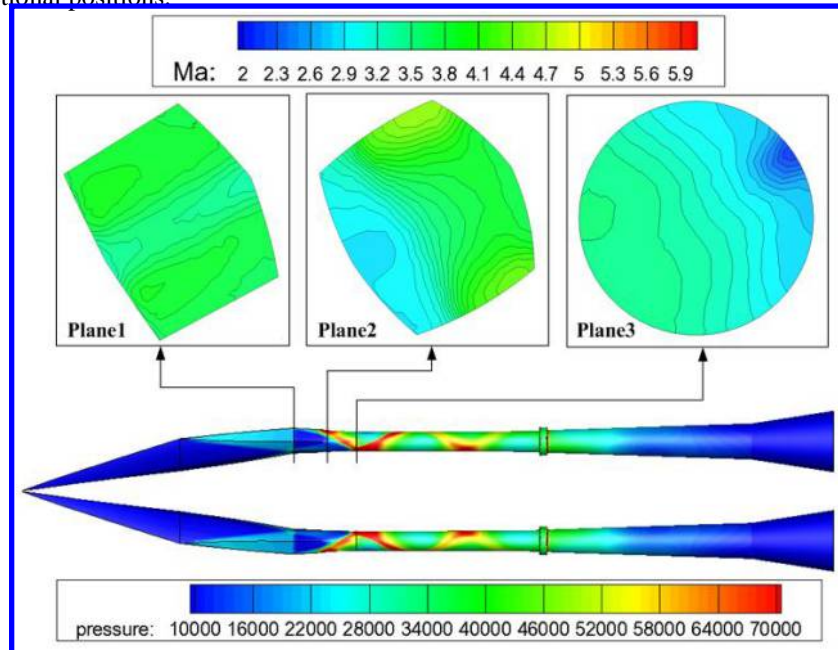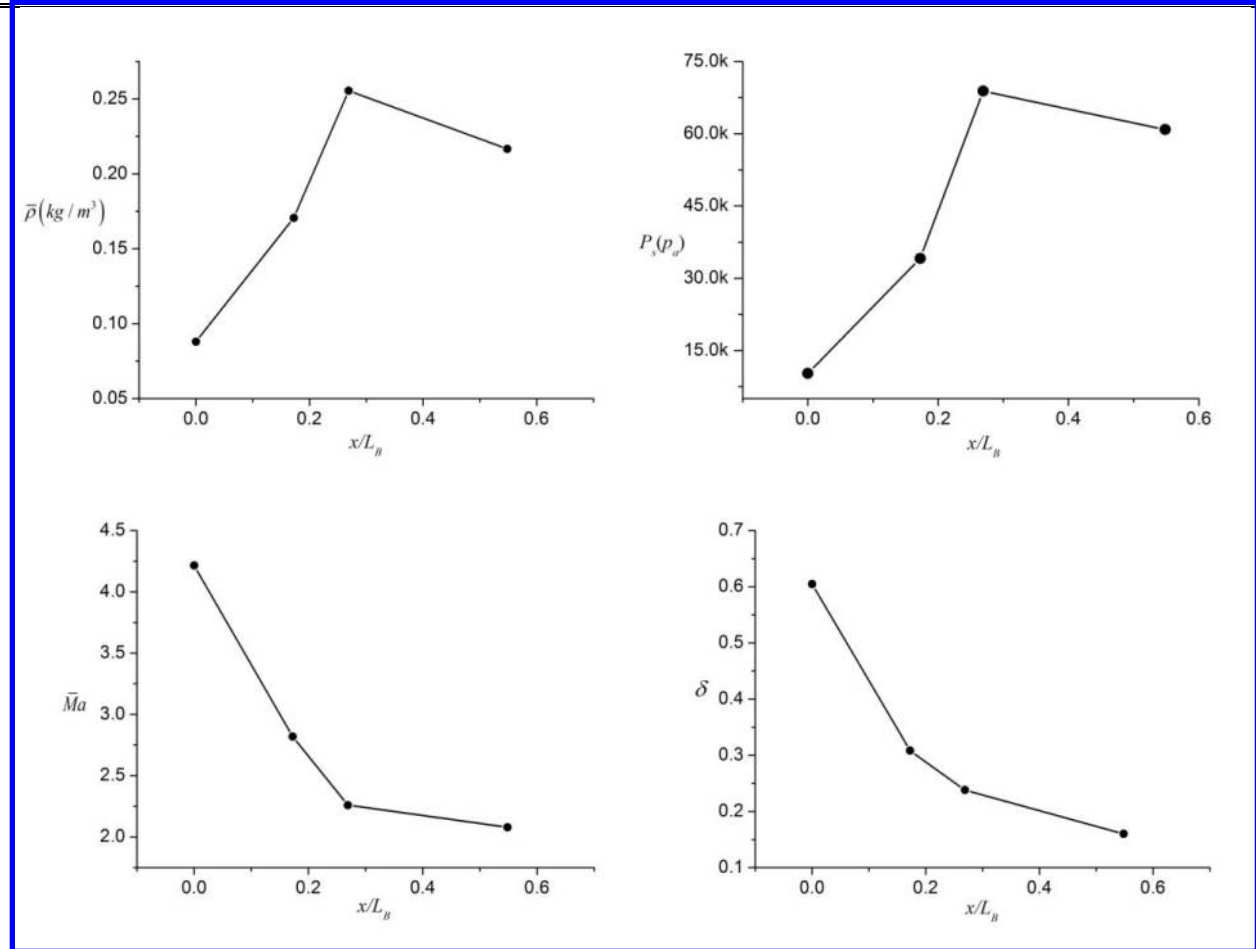
American Institute of Aeronautics and Astronautics

Fig. 12 Mach number and pressure contours on the inner flowpath.

Fig. 13 shows variation curves of the values for the average density $\bar{\rho}$, and the static pressure P_s, the average mach number $\bar{Ma}$, the total pressure recovery coefficient δ at different positions. The horizontal axis of each figure is the relative value by taken the length of the configuration as a reference value. Four positions were selected (Plan1 to Plan4), and the detail description is listed in Table 2. The parameter η_x in Table 2 is the contraction ratio, which is defined by the cross-sectional area at the inlet entrance over the cross-sectional area at the local position. The computational conditions are: $Ma=6$, $H=26$ km, $\alpha=6$ degree.

Table 2 Positions definition and description.

Position	x/L_B	η_x	Position description
Plan1	0	1	Entrance of the inlet
Plan2	0.17	1.88	Entrance of the shrinking section
Plan3	0.27	2.55	Outlet of the shrinking section
Plan4	0.55	2.29	Outlet of the isolator

Fig. 13 Results at different cross-sectional positions.

According to the figures shown in Fig. 13, both the average density and the average pressure gradually increase when the airflow passes over the forebody, the inlet and the shrink section in turn. And in the isolator the values of these two parameters decrease since this part is slight expansion pipe. The values of the average Mach number and the total pressure recovery coefficient decrease. The average Mach number is about 2.08 when the airflow enters into the combustion chamber. The variations of the $\bar{Ma}$ and the δ at four positions with flight the angle of attack ($Ma=6$, $H=26$ km) are shown in Fig. 14. Note from these two figures that both the $\bar{Ma}$ and the δ decreases significantly when the airflow passes over the compression section (from plan1 to plan3). However, the values of the two parameters keep stable essentially in the isolator with the variation of the flight angle of attack, and it is favorable for the operation of the engines.
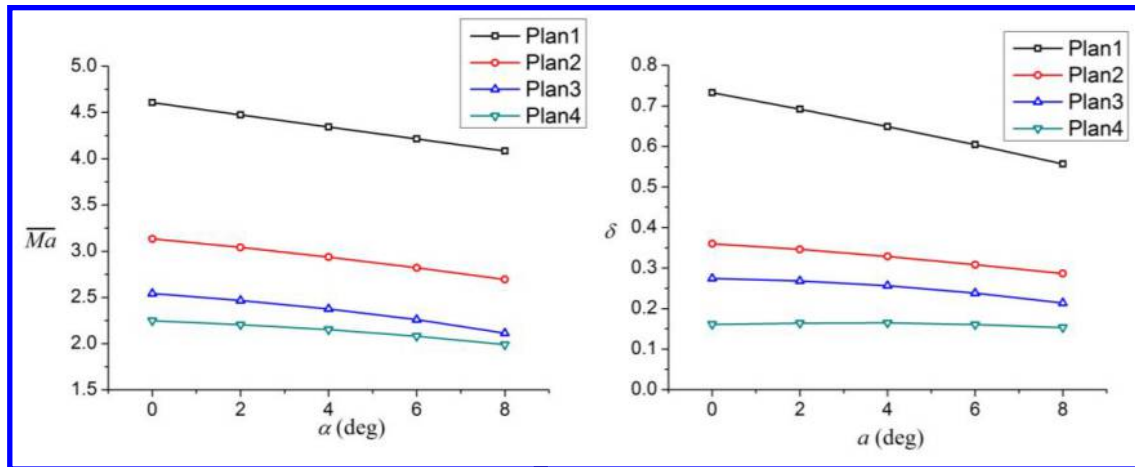
American Institute of Aeronautics and Astronautics

Fig. 14 The variations of the Ma and the δ with flight angle of attack.

B. Performance of the Configuration

Fig. 15 shows the results of aerodynamic parameters in various flight conditions. The Mach number ranges from 4 to 7 and the flight height range from 20 km to 29 km. It is clear that although the values of L/D (from 3.75 to 3.13) exist considerable differences with the variation of the flight Mach number and the height, but the maximal values are all appear at 6 degree of attack. In addition, the lift and the drag coefficients decrease with the Ma/H increase due to the Reynolds number decreases.
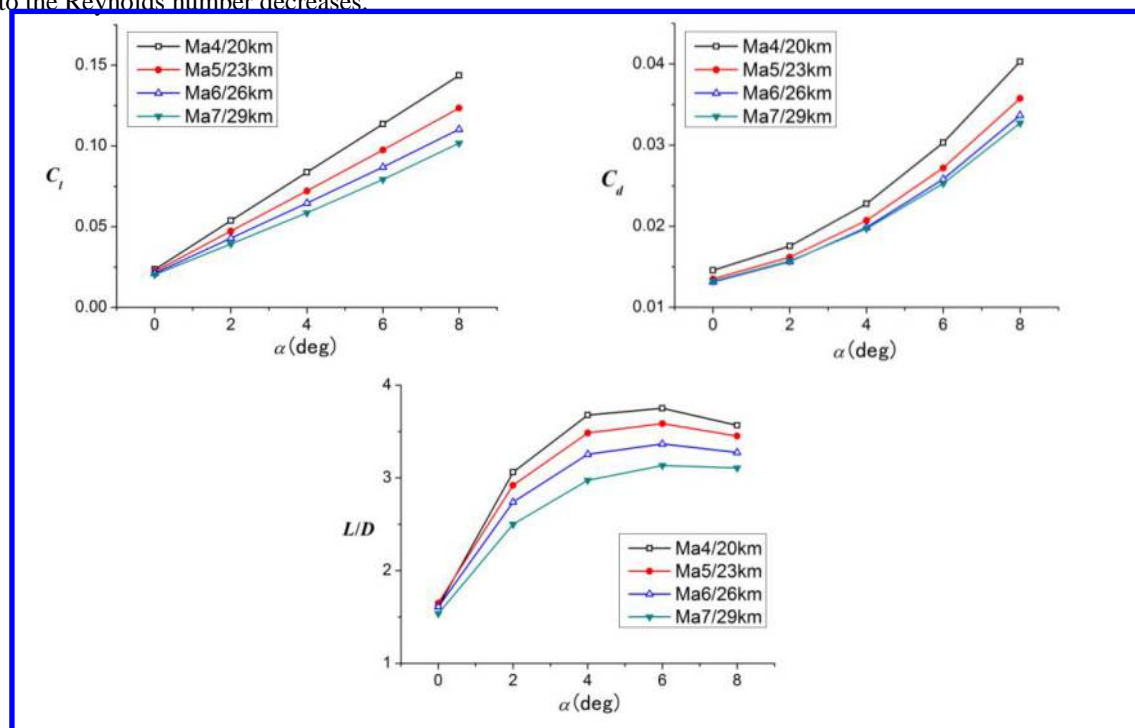

Fig. 15 Aerodynamic parameter comparisons in different flight conditions.

Fig. 16 shows the pressure contour of the lower surface of the vehicle at 0 degree angle of attack. Note from Fig. 16 that the pressure on the stitching surface is apprently high since this part forms a strong compression surface in present design. This phenominon leads that the forebody holds a considerable proportion of the total force. At zero degree angle of attack, the proportion values of lift and drag account for overall are about 22.2% and 28.3%, respectively. Even at six degree angle of attack, they are still 12.8% and 19.6%, respectively. Besides, the lift produced by the wing-body part holds more than 85% of the total lift at six degree angle of attack. It is clear that a shape optimization study of these two parts should be carried on in order to further improve the aerodynamic performance in future.

American Institute of Aeronautics and Astronautics

The variation of pitching moment coefficients (C_{my}) and longitudinal pressure center coefficients (X_{cp}) in all flight conditions are plotted in Fig. 17. The reference point of the pitching moment calculation is the centroid which was near the middle point in the longitudinal direction. The C_{my} decreases with the increase of the angle of attack for all cases, as it is shown in Fig. 17. While the position of the X_{cp} migrates backward slightly. The results indicate that the vehicle is longitudinally stable.
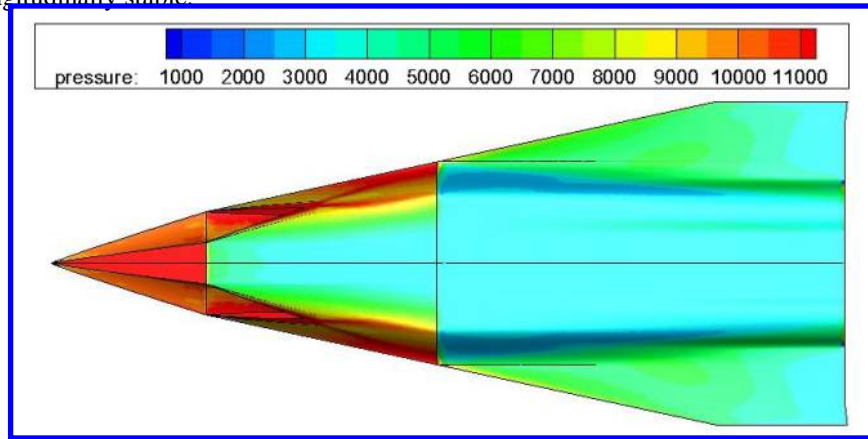

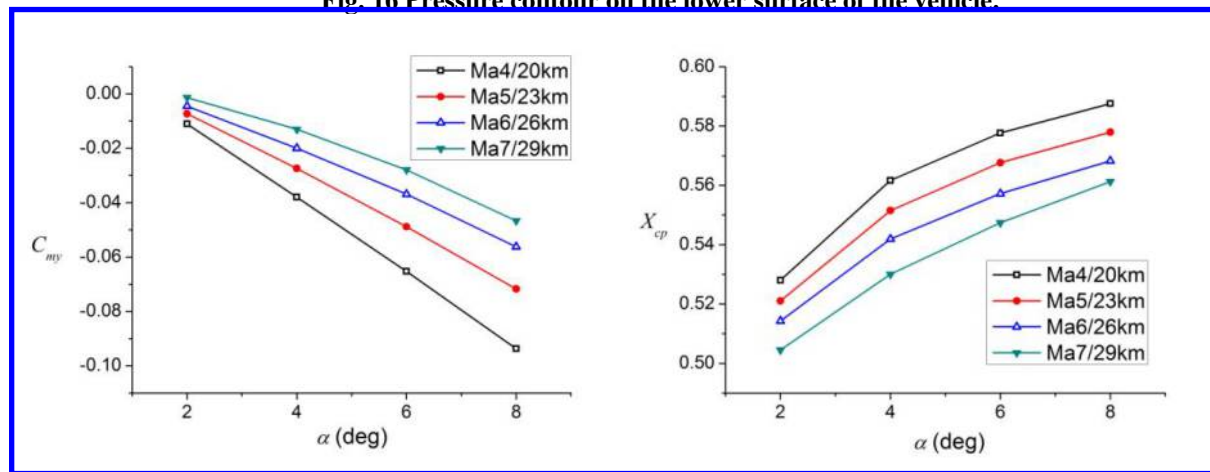Fig. 16 Pressure contour on the lower surface of the vehicle.

Fig. 17 Pitching moment coefficients and longitudinal pressure center coefficients variation in all flight conditions.

V. Conclusions and Discussions

Motivated by developing next generation air-breathing hypersonic airplanes, a novel fore-body design method, which is characterized by rotating and assembling two waverider-based surfaces with linear leading edges, was introduced in this paper; thereby, a conceptual configuration with dual flanking inlets layout was presented. The shape of the configuration comprises of several smooth surfaces, which are determined by cross-sectional and longitudinal profiles. On the basis of components design, a blend-wing-body configuration was designed to aim at aerodynamic drag reduction. In addition, two scramjet engines with side wall compression inlets were also included in the configuration.

By using CFD analysis, the aerodynamic performances were evaluated for the forebody and the whole vehicle in various flight conditions. The results demonstrated that the forebody configuration with dual waverider-based surfaces retains the main advantage of waveriders. Although the flowfield is slightly contaminated due to the existence of the stitching surface, the main region of the flowfield compressed by the forebody is relatively uniform in small flight angle of attack, which can provide a high-quality airflow to the inlet of the scramjet. Moreover, the results also show that the airflow enters the combustion chamber without any choking by using the side wall compression inlet design in all computational conditions. This leads us to believe that the dual-waverider-surfaces-based forebody and the side wall compression inlet integrated design methodology may become a promising scheme for the next generation hypersonic airplanes.

The results of numerical simulation of the whole configuration showed that a relatively high *L/D* was obtained in virtue of a BWB design. In particular, the maximal value of the *L/D* appears at small flight angle of attack (near 6 degree) since a lower bend wing design was adopted by naturally utilizing the height difference between the trailing edge of the forebody and the centerline of engines, which will be propitious to assure stable operation of engines. Even at zero degree angle of attack, the values of the *L/D* are more than 1.5 in all flight conditions on the basis of turbulent model. According to the pressure contour of the vehicle surface and the aerodynamic parameters comparison of different parts, the wing-fuselage part provides most of the lift of the configuration, while the forebody produces considerable drag. Therefore, respective optimization studies should be carried on in next step. Specifically, the leading edge shape of the wing-fuselage should be modified to generate larger lift and the lower stitching surface of the forebody should be deformed to aim at aerodynamic drag reduction.

Unstructured grids was used to alleviate workload of mesh generation in present study. To make up for this deficiency, the meshes near the wall were refined as fine as possible. This is why the total mesh number reaches about 10.65 millions. Anyway, a precise simulation work based on high-quality structured grids as well as wind tunnel experiments validation is necessary in future studies. A preliminary analysis shows that the configuration is longitudinally stable. However, the yawing and rolling stability analysis of the configuration was carried on at present, which is a logical step in future.

The current study mainly focused on the concept developing and a preliminary analysis of the hypersonic airplane with dual waveriders-based forebody. There remains a plenty of realtive problems that should be deeply explored and studied. Besides the shape optimization study and the stability analysis listed above, the present study only aimed at the performance evaluation in hypersonic flight regime. As mentioned previously, the ability of horizontal takeoff and landing is necessary for a hypersonic airplane. On the basis of the present results, the aerodynamic performance of the configuration in low-speed flight conditions and respective multi-point optimization studies should be carried on in future.

Acknowledgments

References

[1] Bertin, J.J., Cummings, R.M., "Fifty Years of Hypersonics: Where We've Been, Where We're Going," *Progress in Aerospace Sciences*, Vol. 39, No. 6-7, 2003, pp. 511-536.

[2] Bowcutt, K.G., Smith, T.R., Kothari, A.P., et al, "The Hypersonic Space and Global Transportation System: A Concept for Routine and Affordable Access to Space," AIAA Paper 2011-2295, 2011.

[3] Lewis, M.J., "A Hypersonic Propulsion Airframe Integration Overview," AIAA Paper 2003-4405, 2003.

[4] Bowcutt, K.G., Kuruvila, G., Grandine, T.A., et al, "Advancements in Multidisciplinary Design Optimization Applied to Hypersonic Vehicles to Achieve Closure," AIAA Paper 2008-2591, 2008.

[5] Tsuchiya, T., Takenaka, Y., Taguchi, H., "Multidisciplinary Design Optimization for Hypersonic Experimental Vehicle," *AIAA Journal*, Vol. 45, No. 7, 2007, pp. 1655-1662.

[6] O'Neill, M.K.L., Lewis, M.J., "Optimized Scramjet Integration on a Waverider," *Journal of Aircraft*, Vol. 29, No. 6, 1992, pp. 1114-1121.

[7] Atamanchuk, T.M., Sislian, J.P., Dudebout, D., "An Aerospace Plane as a Detonation Wave Ramjet/Airframe Integrated Waverider," AIAA Paper 92-5022, 1992.

[8] Blankson, I.M., Hagseth, P., "Propulsion/Airframe Integration Issues for Waverider Aircraft," AIAA Paper 93-0506, 1993.

[9] Molvik, G., Bowles, J., Huynh L., "A Hypersonic Waverider Research Vehicle with Hydrocarbon Scramjet Propulsion: Design and Analysis," AIAA Paper 93-5097, 1993.

[10] O'Neill, M.K.L., Lewis, M.J., "Design Tradeoffs on Scramjet Engine Integrated Hypersonic Waverider Vehicles," *Journal of Aircraft*, Vol. 30, No. 6, 1993, 943-952.

[11] Lewis, M.J., Takashima N., "Waverider Configurations Based on Non-axisymmetric Flow Fields for Engine-Airframe Integration," AIAA Paper 94-0380, 1994.

[12] Lewis, M.J., Takashima N., "Wedge-Cone Waverider Configuration for Engine-Airframe Integration," *Journal of Spacecraft and Rockets*, Vol. 32, No. 5, 1995, pp.1142-1144.

[13] Haney, J.W., Beaulieu, W.D., "Waverider Inlet Integration Issues," AIAA Paper 94-0383, 1994.

[14] Haney, J.W., Beaulieu, W.D., "Waverider Nozzle Integration Issues," AIAA Paper 95-0847, 1995.

[15] Takashima N., Lewis, M.J., "Engine-Airframe Integration on Osculating Cone Waverider-Based Vehicle," AIAA Paper 96-2551, 1996.

[16] Lobbia, M. A., Suzuki, K., "Numerical Investigation of Waverider-Derived Hypersonic Transport Configurations," AIAA Paper 2003-3804, 2003.

[17] Cui, K., Yang, G.W., "Conceptual Design of Hypersonic Vehicles with Large Capacity and High Aerodynamic Performance," AIAA Paper 2009-7400, 2009.

[18] Lobbia, M.A., Suzuki, K. "Multidisciplinary Design Optimization of Hypersonic Transport Configurations using Waveriders," AIAA Paper, 2014-2359 2014.

[19] Sobieczky, H., Dougherty, F. C., Jones, K. D., "Hypersonic Waverider Design from Given Shock Waves," in *Proceedings of the First International Hypersonic Waverider Symposium,* University of Maryland, College Park, MD, Oct. 17-19, 1990.

[20] O'Brien, T.F., Lewis, M.J., "Rocket-Based Combined-Cycle Engine Integration on an Osculating Cone Waverider Vehicle," *Journal of Aircraft*, Vol. 38, No. 6, 2001, pp. 1117-1123.

[21] Javaid, K.H., Serghides, V.C., "Thrust-Matching Requirements for the Conceptual Design of Hypersonic Waverider Vehicles," *Journal of Aircraft*, Vol. 42, No. 4, 2005, pp.1055-1064.

[22] Javaid, K.H., Serghides, V.C., "Airframe–Propulsion Integration Methodology for Waverider-Derived Hypersonic Cruise Aircraft Design Concepts," *Journal of Spacecraft and Rockets*, Vol. 42, No. 4, 2005, pp.663-671.

[23] Tang, M., Chase, R.L., "The Quest for Hypersonic Flight with Air-Breathing, Propulsion," AIAA Paper 2008-2546, 2008.

[24] Walker, S., Tang, M., Morris, S., et al, "Falcon HTV-3X – A Reusable Hypersonic Test Bed," AIAA Paper 2008-2544, 2008.

[25] Cui, K., Hu, S.C., Li, G.L., et al, "Conceptual design and aerodynamic evaluation of hypersonic airplane with double flanking air inlets," *Science China Technology Science*, Vol.56, No.8, 2013, pp.1980-1988.

[26] Cui, K., Zhao, D.X., Yang, G.W., "Waverider Configurations Derived from General Conical Flowfields," *Acta Mechanica Sinica*, Vol.23, No.3, 2007, pp.247-255.

[27] Cui, K., Yang, G.W., "The Effect of Conical Flowfields on the Performance of Waveriders at Mach 6," *Chinese Science bulletin*, Vol.52, No.1, 2007, pp.57-64.

[28] Sabean, J.W., Lewis, M.J., Mee, D. et al, "Performance Study of a Power Law Star Body," AIAA Paper 1998-1617, 1998.